The Cryosphere, 20, 6883–6898, 2026
https://doi.org/10.5194/tc-20-6883-2026
© Author(s) 2026. This work is distributed under
the Creative Commons Attribution 4.0 License.

The Cryosphere Open Access EGU

An accurate present-day model of the Antarctic ice sheet is necessary but insufficient for an accurate projection of its future evolution

Constantijn J. Berends[1], **Jorge A. Bernales**[2], **Erwin Lambert**[3], **and Roderik S. W. van de Wal**[1,3,4]

[1]Institute for Marine and Atmospheric research Utrecht (IMAU), Utrecht University, Utrecht, the Netherlands
[2]Danish Meteorological Institute (DMI), Copenhagen, Denmark
[3]Royal Dutch Meteorological Institute (KNMI), De Bilt, the Netherlands
[4]Department of Physical Geography, Faculty of Geosciences, Utrecht University, Utrecht, the Netherlands

Correspondence: Constantijn J. Berends (c.j.berends@uu.nl)

Received: 7 July 2026 – Discussion started: 15 July 2026
Revised: 26 October 2026 – Accepted: 4 November 2026 – Published: 24 November 2026

Abstract. Accelerated retreat of the Antarctic ice sheet dominates both the magnitude of, and the uncertainty in, high-end sea-level projections. One frequently cited caveat in the computational models used to create these projections is that many of them poorly represent the observed present-day state of the ice sheet. Following the thought that a model should accurately represent the present before it can be expected to accurately represent the future, there have been discussions in the ice-sheet modelling community to weight or even exclude individual models from ensemble studies based on how well they reproduce present-day observations. In this study, we create a wide ensemble of realisations with a numerical ice-sheet model under different parametric assumptions, utilising inverse methods to ensure every realisation reproduces snapshot observations of the present-day geometry, velocity, and thinning rates of the Antarctic ice sheet to a degree that is comparable with the most recent ISMIP6 ensemble. Our model realisations project anything between -0.3 and $+1.5$ m of sea-level contribution (SLC) by 2300, with the sea-level rate at that time varying from -0.7 to $+9.7\,\mathrm{mm\,yr^{-1}}$. There is no clear relation between the degree to which these model realisations reproduce snapshot observations of the present-day ice sheet, and the amount of SLC they project. The main factors contributing to the wide variance in projected SLC are the sliding law and the distribution of the roughness of the substrate. Since these quantities are typically derived by inversion from observations of the ice flow, they can only be known as accurately as other processes affecting the flow, such as subglacial hydrology, ice damage, and calving. This implies that weighting or excluding models from ensemble studies based only on their agreement with snapshot observations of the present-day ice sheet might not be a wise choice. Instead, comparing to temporal observations, or to novel observations of the ice sheet's subsurface, might be more helpful to reduce the uncertainty in Antarctica's future contribution to sea-level rise.

1 Introduction

Sea-level rise caused by mass loss of the Greenland and Antarctic ice sheets is both one of the most worrisome, and one of the most uncertain long-term consequences of anthropogenic climate change (van de Wal et al., 2022). At present, mass loss from the Antarctic ice sheet on average contributes approximately $0.41\,\mathrm{mm\,yr^{-1}}$ to the global mean sea-level rate (Otosaka et al., 2023; Seroussi et al., 2024), but several instabilities are hypothesised to exist within the ice-sheet system that could potentially cause this rate to accelerate strongly in the future. Particularly, the marine ice-sheet instability (Weertman, 1974) and the marine ice-cliff instability (DeConto and Pollard, 2016) have been identified as possible drivers of rapid mass loss in the future. The physical processes underlying these instabilities, which involve both fundamental ice dynamics and their interaction with the subglacial substrate and ocean, remain poorly understood, leading to large uncertainties in estimates of the future

Antarctic sea-level contribution. For example, the most recent concerted international effort to project the future evolution of the ice sheet using numerical ice-sheet models, the Ice Sheet Model Intercomparison Project for CMIP6 (ISMIP6; Seroussi et al., 2024), estimated that, under the high-warming SSP5-8.5 scenario, the Antarctic ice sheet could contribute between -2.1 and $+8.4\,\mathrm{mm\,yr^{-1}}$ by 2100 (with negative numbers indicating a sea-level drop), causing global mean sea level to increase by -0.2 to $+0.3$ m with respect to 2014. By 2300, the sea-level rate is estimated to lie between -2.1 and $+28.5\,\mathrm{mm\,yr^{-1}}$, and the sea-level rise between -0.6 and $+4.5$ m. The idea of a negative future Antarctic SLC is generally seen as unlikely, yet 10 out of the 16 models in the ISMIP6 ensemble produced a negative SLC in at least some of their projections. Rather than discarding such results as statistical outliers, we must therefore accept the fact that ice-sheet models currently cannot agree on the sign of the future Antarctic contribution to sea level. Reducing this large uncertainty is arguably the most important topic today in numerical glaciology.

Seroussi et al. (2024) provide some analysis of the variance in the ISMIP6 model ensemble. They find that the choice of ice-sheet model dominates the variance in sea-level projections until the year 2100; after that, the choice of general circulation model (GCM) used to generate the atmospheric and oceanic forcing, becomes a significant secondary term. It is important to note here that the choice of basal melt forcing, which is well known to be a strong control on Antarctic mass loss (e.g. Burgard et al., 2022; Berends et al., 2023a), and the representation of which varies greatly between models (Lambert and Burgard, 2025) is, in the work by Seroussi et al. (2024) included in the "choice of ice-sheet model". However, the general notion that differences between different ice-dynamical models cause strong differences in the modelled sea-level rise is well-supported by other studies (e.g. Cornford et al., 2020; Sun et al., 2020; Berends et al., 2023b; Coulon et al., 2025).

These large differences between ice-sheet models reflect our incomplete understanding of several crucial physical processes governing the Antarctic ice sheet system – particularly processes occurring beneath the ice surface. Since the dawn of the satellite era, the ice-sheet surface is observed at a relatively high spatial and temporal resolution. However, conditions in the ice interior and at the base are generally poorly constrained. Both the current state and the future evolution of the ice sheet are strongly affected by the [bulk] viscosity of the ice (Getraer and Morlighem, 2025), the roughness of the subglacial substrate (Sun et al., 2020), the subglacial topography (Castleman et al., 2022), the state of the subglacial hydrological system (Kazmierczak et al., 2022), and the conditions of the ocean and the concomitant melt rates in the cavities underneath the ice shelves (Burgard et al., 2022; Berends et al., 2023a), and yet direct observations or measurements are scarce to the point of not existing at all. Instead, many of these quantities are often derived by inversion from observations at the ice surface (e.g. Arthern and Gudmundsson, 2010; Pollard and DeConto, 2012; van Pelt et al., 2013; Arthern et al., 2015). However, since the relation between conditions at the base and conditions at the surface is often strongly non-local, non-linear, and diffusive (Gudmundsson and Raymond, 2008), inverting for basal conditions from surface observations is not trivial, and generally leads to large uncertainties, and often to non-unique solutions. Some models use a different approach, attempting to constrain the phase space of possible parameter values from a palaeo perspective, reproducing ice-sheet evolution in the geological past (e.g. Lecavalier and Tarasov, 2025). However, we are not aware of any models using this approach to constrain the spatial distribution of bed roughness.

Another source of uncertainty stems from the fact that Antarctica is at present losing mass. van den Akker et al. (2025) showed that neglecting this imbalance and instead initialising an ice-sheet model to a steady state at the present day, overestimates the stability of the ice sheet. They showed that initialising their model to accurately reproduce the observed thinning rates leads to the inevitable loss of almost all grounded ice in the Amundsen Sea basin within the next two millennia – even without additional climate forcing, implying that we are already committed to the future collapse of this sector. Since many ice-sheet models in the ISMIP6 ensemble (Seroussi et al., 2024) are initialised to a steady state, and thereby potentially biased towards a lower SLC, it is conceivable that this explains some of the spread in the model ensemble.

Based on these findings, as well as earlier exploratory work (e.g. Goelzer et al., 2018; Seroussi et al., 2019), there is now a tendency for studies on future ice-sheet evolution to also report on the accuracy of their modelled present-day ice sheet, including the observed mass trend (e.g. Coulon et al., 2024, 2025; Klose et al., 2024; Seroussi et al., 2024). This accuracy is typically quantified in terms of some manner of integrated error (often a simple root-mean-square) with respect to "snapshot" observations of the ice surface: satellite-derived, time-averaged, gridded data, which can be conveniently compared to the output of most numerical ice-sheet models. However, since the basal processes that are thought to govern the future evolution of the ice sheet cannot be easily constrained from observations of the ice surface (Gudmundsson and Raymond, 2008), comparing to such snapshot observations alone is not a guarantee for improving the accuracy of the future SLC projected by the ice-sheet model.

In this study, we demonstrate that the degree of agreement between an ice-sheet model, and observations of the ice-sheet surface (even when thinning rates are included) is not related to the amount of future SLC projected by the model. We construct an ensemble of realisations of the Utrecht Finite Volume Ice-Sheet Model (UFEMISM v2.0; Berends et al., 2025), sampling the uncertainty in the basal processes governing ice-sheet evolution. By initialising each realisation separately using an inverse approach, we ensure that all of

them reproduce satellite observations of the ice-sheet surface to a degree that is comparable with the recent ISMIP6 ensemble by Seroussi et al. (2024). We then integrate these model realisations for two centuries into the future under SSP5-8.5 climate/ocean forcing. We find no relation between the "quality" of the initial state of each model realisation, and the projected SLC by 2300. Instead, we find that the projected SLC depends most strongly on the choice of sliding law, and the distribution of bed roughness. We show that, due to compensating effects, any of these choices can yield a model realisation that "fits" the surficial observations.

2 Model description

2.1 Overview

A detailed description of UFEMISM v2.0, including the governing equations, their discretisation, the basics of the mesh generation toolbox, and the parallelisation scheme, is provided by Berends et al. (2025). Briefly, UFEMISM solves the momentum balance (approximated in this study by the depth-integrated viscosity approximation, DIVA; Goldberg, 2011) on a dynamic adaptive mesh, which is adapted to the evolving ice geometry over the course of a simulation. The mesh is generated according to a set of user-provided resolutions for different regions of the ice-sheet system, such as the ice sheet, the ice shelf, the grounding line, and the ice front. By using a high resolution around the grounding line (down to 1 km in the simulations presented here) and a coarser resolution elsewhere, the computational efficiency is greatly increased. Different sliding laws are available for the user to choose from, including the commonly used Weertman-type (power) law, Coulomb-type (velocity-independent friction) law, and Zoet-Iverson (hybrid) law. UFEMISM scales the basal friction coefficient in partially grounded cells with the grounded fraction of each cell, which results in a good representation of grounding-line migration even at resolutions of tens kilometers (Berends et al., 2025). UFEMISM uses an adaptive time step, which is calculated using a predictor-corrector scheme based on the one developed for Yelmo (Robinson et al., 2020), which was in turn based on the work by Cheng et al. (2017). Conservation of mass is solved using a finite-volume scheme with a discretisation scheme that is semi-implicit in time (defining the ice thickness at time step $n+1$, but the ice velocity at time step n), though a simpler explicit scheme is included too.

2.2 Sliding laws

In this study, we use two different sliding laws. The first is a classic Weertman-type power law (Weertman, 1957):

$$\beta = C_{\mathrm{w}} \mathbf{u}_{\mathrm{b}}^{\frac{1}{m}-1}. \tag{1}$$

Here, β is the (non-linear, velocity-dependent) basal friction coefficient, which relates the basal sliding velocity $\mathbf{u}_{\mathrm{b}}$ to the basal shear stress τ_{b} as $\tau_{\mathrm{b}} = \beta \mathbf{u}_{\mathrm{b}}$. C_{w} is the (flow-independent) bed roughness, and m is the exponent of the power law.

The second option is the Zoet-Iverson law (Zoet and Iverson, 2020):

$$\beta = N \tan\phi \left(\frac{u_{\mathrm{b}}}{u_{\mathrm{b}} + u_0} \right)^{\frac{1}{p-1}}. \tag{2}$$

Here, N is the (effective) overburden pressure, ϕ is the bed roughness (expressed here as the till friction angle), $u_0 = 200\,\mathrm{m\,yr^{-1}}$ is the transition velocity, and $p = 5$ is the exponent for the power-law part of the law. For slow-moving ice, this law behaves like a power law, with the basal shear stress vanishing as the basal velocity approaches zero. For fast-flowing ice streams, the friction asymptotes to the Coulomb limit $N \tan\phi$. In this sense, the Zoet–Iverson law is similar to the hybrid sliding laws proposed by Schoof (2005) and Tsai et al. (2015), which were used in the MISMIP+ experimental protocol (Asay-Davis et al., 2016).

2.3 Bed roughness: inversion by nudging

The approach of iteratively "nudging" the subglacial bed roughness to achieve a stable ice geometry that is close to some target geometry, was first presented by Pollard and DeConto (2012). During a forward simulation, the modelled ice thickness is compared to the target; if the ice is too thin, then it is assumed that too much ice is flowing away, and the bed roughness is increased to remedy this, and vice versa if the ice is too thick. Lipscomb et al. (2021) improved on this scheme by including a term with the thinning rate $\mathrm{d}H/\mathrm{d}t$ in the equation, which damps spurious oscillations and greatly improves the stability and rate of convergence. Berends et al. (2023b) then adapted this work by using the ice velocity instead of the thinning rate, and by averaging the thickness and velocity errors over the flowline passing through each cell, again improving the stability and convergence. In this study, we included two variants of the flowline-averaged nudging scheme by Berends et al. (2023b) in UFEMISM, and a purely local scheme intended to copy that used in CISM.

It is contested how (dis)similar nudging schemes like the one used here are to the more formal adjoint-based inversion methods used in e.g. Elmer/ice (Gagliardini et al., 2013) and ISSM (Larour et al., 2012), which typically explicitly define a cost function to be minimised. Regardless, nudging methods have been shown to be reliable tools to obtain good representations of the present-day observed Greenland and Antarctic ice sheets across different ice-sheet models (e.g. CISM, Lipscomb et al., 2021; IMAU-ICE, Berends et al., 2023b; UFEMISM, Berends et al., 2025).

Table 1. Constants in the H–u scheme.

Parameter	Value	Units
u_0	450	$\mathrm{m\,yr^{-1}}$
H_0	100	m
t_s	200	years
L	2000	m
$\tau_\mathrm{Zoet-Iverson}$	50	years
τ_Weertman	5000	years
u_s	3000	$\mathrm{m\,yr^{-1}}$
H_s	300	m

2.3.1 H–u nudging scheme

The first scheme, hereafter called the "H–u scheme", is very similar to the scheme presented by Berends et al. (2023b), using the ice thickness and velocity errors to nudge the bed roughness C:

$$\frac{\partial C}{\partial t} = -C\left[\left(\frac{f_\mathrm{u}(\Delta u)}{u_0} + \frac{f_\mathrm{d}(\Delta u)}{u_0} + \frac{f_\mathrm{u}(\Delta H)}{H_0}\right)\frac{R}{t_\mathrm{s}} - \frac{L^2}{\tau}\nabla^2 C\right], \quad (3)$$

$$R = \min\left(1, \max\left(0, \frac{uH}{u_\mathrm{s} H_\mathrm{s}}\right)\right). \quad (4)$$

Here, C is the "generic bed roughness", which depends on the choice of sliding law. In the case of the Weertman sliding law, it is identical to C_W in Eq. (1); for the Zoet–Iverson law, it is identical to ϕ in Eq. (2). The functions $f_\mathrm{u}(g(x,y))$ and $f_\mathrm{d}(g(x,y))$ average a function $g(x,y)$ (in this case, either the ice thickness error $\Delta H(x,y)$ or the ice velocity error $\Delta u(x,y)$) over, respectively, the upstream and downstream half-flowline passing through the point $[x,y]$ (see Berends et al., 2023b). u is the ice surface speed ($u = |\mathbf{u_s}|$), H is the ice thickness, and Δu, ΔH are the respective differences between the modelled values of these quantities, and their target values (either from observations, or from another model simulation). u_0, H_0, t_s, L, τ, u_s, and H_s are all constants (see Table 1). Note that τ has different values for the Zoet–Iverson and Weertman sliding laws, reflecting the different units of the bed roughness in these laws. Compared to the version used by Berends et al. (2023b), the term with the Laplacian $\nabla^2\phi$ is new, replacing the Gaussian smoothing functions in their Eq. (9) to yield a slightly more numerically stable regularisation approach. This is inspired by recent experimental work with the Community Ice Sheet Model.

Essentially, this approach integrates a parabolic partial differential equation for C through time to find the steady-state solution. Although there is, to the best of our knowledge, no formal proof for the conditions under which this scheme is guaranteed to converge/diverge, Berends et al. (2023b) showed that it converges for a uniform initial guess ($C(x,y,t=0) = C_0$). In practice, we find that a better initial guess leads to much faster convergence. Particularly, using the steady state resulting from a lower-resolution simulation (which can be run much faster) is a convenient approach, since the remaining errors are typically only the short-wavelength terms, which diffuse much faster.

Table 2. Constants in the H–$\mathrm{d}H/\mathrm{d}t$ scheme.

Parameter	Value	Units
t_s	150	years
c_1	200	m
c_2	0.7	$\mathrm{m\,yr^{-1}}$

Table 3. Constants in the H–$\mathrm{d}H/\mathrm{d}t$-local scheme.

Parameter	Value	Units
H_0	200	m
τ	200	years
L	40	m

2.3.2 H–$\mathrm{d}H/\mathrm{d}t$ nudging scheme

The second nudging scheme used in this study, hereafter called the "H–$\mathrm{d}H/\mathrm{d}t$" scheme, replaces the velocity error term in Eq. (3) with a term based on the modelled thinning rate $\partial H/\partial t$:

$$\frac{\partial C}{\partial t} = -\frac{C}{t_\mathrm{s}}\left[\frac{f_\mathrm{u}(\Delta H) - \frac{1}{4} f_\mathrm{d}(\Delta H)}{c_1} + \frac{f_\mathrm{u}\left(\frac{\partial H}{\partial t}\right) - \frac{1}{4} f_\mathrm{d}\left(\frac{\partial H}{\partial t}\right)}{c_2}\right]. \quad (5)$$

Here, t_s, c_1, c_2 are constants (see Table 2). Note that Eq. (5) does not include the Laplacian of C; instead, regularisation of the solution is achieved following Berends et al. (2023b), applying a Gaussian smoothing filter with a radius of 5000 m to $\frac{\partial C}{\partial t}$ before calculating $C\left(t^{n+1}\right)$.

2.3.3 H–$\mathrm{d}H/\mathrm{d}t$-local nudging scheme

The last nudging scheme, hereafter called the "H–$\mathrm{d}H/\mathrm{d}t$-local" scheme, is based directly on that of CISM, aiming to provide a closer comparison to the results by van den Akker et al. (2025):

$$\frac{\partial C}{\partial t} = -C\left[\frac{\Delta H}{H_0 \tau} + \frac{2}{H_0 \frac{\partial H}{\partial t}} - \frac{L^2}{\tau \nabla^2 C}\right]. \quad (6)$$

The values of the constants in Eq. (6) are listed in Table 3.

2.4 Ocean conditions and sub-shelf melt: parameterisation or inversion

2.4.1 World Ocean Atlas + quadratic ocean forcing

In this work, we used three different methods to determine the sub-shelf melt rates during the initialisation. The first method calculated the sub-shelf melt rates from the ocean thermal forcing (World Ocean Atlas; Locarnini et al., 2019)

using a simple local quadratic dependence, following Favier et al. (2019; their Eq. 4):

$$m = -c_{\text{spy}}\gamma \,\text{sgn}\,(\Delta T)\left(\frac{\rho_{\text{sw}} c_{\text{p,sw}} \Delta T}{\rho_{\text{i}} L_{\text{fus,i}}}\right)^2. \tag{7}$$

Here, $\Delta T = T_{\text{sw}} - T_{\text{f}}$ is the thermal forcing (defined as the difference between the local seawater temperature T_{sw} at the ice shelf draft, and the pressure/salinity-dependent freezing temperature T_{f}), and $\text{sgn}\,(\Delta T)$ is the sign of the thermal forcing (so that a negative thermal forcing will correctly result in refreezing rather than melt). The constants c_{spy} (the number of seconds per year, to keep the units of γ consistent with existing literature, while still providing the melt rate m in meters per year), ρ_{sw}, $c_{\text{p,sw}}$, ρ_{i}, and $L_{\text{fus,i}}$ are given in Table 4. The local and non-local quadratic parameterisations by Favier et al. (2019) are currently the most widely-used zero-dimensional basal melt parameterisations in ice-sheet models.

We used the ISMIP6-Ant2300 present-day ocean temperature and salinity (Seroussi et al., 2024) to force our quadratic melt parameterisation. This dataset is based on the World Ocean Atlas 2018 (WOA; Locarnini et al., 2019; Zweng et al., 2019), which is extrapolated into the sub-shelf cavities using the ISMIP6 protocol (Jourdain et al., 2020).

2.4.2 Nudged World Ocean Atlas + quadratic ocean forcing

Our second method extends this approach by iteratively nudging the ocean temperature in the sub-shelf cavity, to minimise the difference between the modelled and observed thickness of the ice shelves. Since ocean conditions in the sub-shelf cavities are poorly constrained, and the extrapolated World Ocean Atlas temperatures have a large error, this approach essentially attempts to a posteriori reconstruct what these temperatures should look like, in order to produce a stable ice shelf with a thickness close to the snapshot target. All of this is, of course, under the assumption of the quadratic relation between ocean temperature and basal melt rates; if a different basal melt law is used, different ocean temperatures will be produced by the nudging scheme. The ocean temperatures are nudged on a per-grid-cell basis, with some smoothing applied to prevent spurious horizontal temperature gradients.

2.4.3 Inverted melt rates

In our third scheme, we bypass ocean conditions altogether, and instead directly nudge the basal melt rates on a per-grid-cell basis:

$$\frac{\partial m}{\partial t} = c_1 \Delta H + c_2 \frac{\partial H}{\partial t} \tag{8}$$

Here, m is the sub-shelf melt rate, and c_1 and c_2 are constants (see Table 5). The $\mathrm{d}H/\mathrm{d}t$ term helps to stabilise the solution, preventing spurious oscillations.

This approach is included to serve as a "sanity check", verifying that the melt rates that are required to maintain a stable ice geometry are not wholly unphysical (which would indicate problems in the ice dynamics and/or the surface mass balance). It also has the advantage of producing an initial state that is, at least over the shelves, closer to observations than can generally be achieved when using a physical melt parameterisation (i.e. within a meter of the observed ice thickness). A downside is that this initial state cannot be meaningfully used for projections, as it is very difficult to adapt the resulting spatial distribution of melt to an evolving ice geometry. The experiments presented in Appendix A are an exception, as there the ice-sheet retreat is forced by calving, and no shelves exist at all.

2.5 Sub-grid melt parameterisation

UFEMISM offers different ways to treat basal melt near the grounding line. Following the nomenclature proposed by Leguy et al. (2021), these are called the "flotation criterion melt parameterisation" (FCMP) and the "partial melt parameterisation" (PMP). FCMP implies that the basal melt rate is applied only to grid cells whose grid point is floating, with no scaling; in the PMP scheme, this melt rate is scaled with the floating fraction of the grid cell (even when the grid point is grounded).

2.6 Matching the observed thinning rates

Following the approach by van den Akker et al. (2025), we subtract the observed ice thinning rates (Smith et al., 2020) from the prescribed surface mass balance (SMB) during the initialisation. This prevents biases in the friction or basal melt rates, where the model would otherwise attempt to counteract the thinning by artificially overestimating the friction, resulting in a bias towards a too stable ice sheet. When the initialisation is finished and the projection starts, we stop subtracting the thinning rates from the SMB, so that the ice sheet will immediately thin at (approximately) the observed rates.

3 Methodology

3.1 Initialisation and forcing

We have used UFEMISM v2.0 to produce an ensemble of initial states for simulations of the Antarctic ice sheet. The ensemble members differ in the sliding law (3 options), the nudging scheme for the bed roughness (3 options), the calculation of the basal melt (3 options), the treatment of basal melt around the grounding line (2 options), and the resolution at the grounding line (6 options). The different options are listed in Table 6. All these realisations used the same constant present-day surface mass balance, calculated using RACMO2.3p2 at a native resolution of 27 km, downscaled to a resolution of 2 km, and averaged over the period 1979–

Table 4. Constants in the quadratic basal melt parameterisation.

Parameter	Description	Value	Units
c_{spy}	Number of seconds per year	3.155694336×10^7	$\mathrm{s\,yr^{-1}}$
ρ_{sw}	Density of seawater	1.027×10^3	$\mathrm{kg\,m^{-3}}$
$c_{\mathrm{p,sw}}$	Specific heat of seawater	3.974×10^3	$\mathrm{J\,kg^{-1}\,K^{-1}}$
ρ_{i}	Density of ice	9.1×10^2	$\mathrm{kg\,m^{-3}}$
$L_{\mathrm{fus,i}}$	Heat of fusion of ice	3.335×10^5	$\mathrm{J\,kg^{-1}}$

Table 5. Constants in the sub-shelf melt nudging scheme.

Parameter	Value	Units
c_1	0.003	$\mathrm{yr^{-2}}$
c_2	0.03	$\mathrm{yr^{-1}}$

2021 (Noël et al., 2023). Note that the grounding-line resolution indicates the maximum allowed distance between vertices; in practice, the average distance between them (the "effective" resolution) is typically about 20 % smaller.

The initialisations at different resolutions are performed sequentially: first, the 20 km initialisation is run for 40 000 years, starting with a uniform, high value for the bed roughness. Then, the 10 km version is run for 20 000 years, starting with the final bed roughness distribution of the 20 km version as its initial guess to speed up the convergence. Then, the 5 km version is run for 10 000 years, starting with the final bed roughness of the 10 km version, etc. These durations are chosen so that the simulated sea-level drift at the end of the simulation is below 1 cm per century, which we find to be acceptably stable.

We have performed a single future projection under SSP5-8.5 for each of these initial states, except for those where the basal melt rate was inverted, rather than derived from (nudged) ocean temperatures (as the resulting melt distribution is very difficult to adapt to an evolving ice geometry). Each of the projections used the same climate and ocean forcing, which was derived by taking the mean of the 4 GCM projections used for this experiment in ISMIP6 Ant2300 (Seroussi et al., 2024). For this ensemble mean, the anomalies with respect to the 1979–2021 baseline period were calculated, and added to the (higher resolution, less biased) present-day climate calculated with the regional climate model RACMO2.3p2 by Noël et al. (2023) in case of the surface mass balance, and to the baseline ocean state (either the WOA, or the nudged version thereof) in case of the basal mass balance. We did not include calving, nor any forced shelf collapse such as was done in the work by Seroussi et al. (2024). However, while we did not allow the calving front to advance beyond its present-day position, it could still retreat because of basal melt. Glacial isostatic adjustment was not included. All projections were initialised in the year 2014 and were run until the year 2300. Note that our choice of using the ensemble mean of the four different GCMs that were used in ISMIP6, means that we cannot directly compare the projected SLC to the models in that ensemble, due to the difference in climate forcing.

3.2 Initial state quality quantification

We quantify the quality of our initial state in terms of the root-mean-square error (RMSE) in the ice thickness, and the ice surface speed. For the ice thickness, we compare to BedMachine Antarctica v3 (Morlighem et al., 2017), while for the ice surface speed, we compare to MEaSUREs Antarctica v2 (Rignot et al., 2011). These RMSE's are computed on UFEMISM's native unstructured triangular grid, weighting the error at each grid cell by that grid cell's area:

$$\mathrm{RMSE}(H) = \sqrt{\frac{\sum_i \left(H^i_{\mathrm{UFE}} - H^i_{\mathrm{BedMachine}}\right)^2 A^i}{\sum_i A^i}}, \tag{9}$$

$$\mathrm{RMSE}(u) = \sqrt{\frac{\sum_j \left(u^j_{\mathrm{UFE}} - u^j_{\mathrm{MEaSUREs}}\right)^2 A^j}{\sum_j A^j}}. \tag{10}$$

Here, the errors between UFEMISM's ice thickness H_{UFE} and BedMachine's ice thickness $H_{\mathrm{BedMachine}}$ are summed over the mesh vertices i, while the errors between UFEMISM's ice surface speed u_{UFE} and the MEaSUREs ice surface speed u_{MEaSUREs} are summed over the mesh triangles j, reflecting UFEMISM's thickness/velocity staggering. Optionally, we can compute these sums over individual drainage basins instead of over the entire Antarctic ice sheet, to quantify the model's ability to reproduce the observed ice sheet in a particular area.

To be able to study the relation between the "quality" of a model's initial state, and its future evolution, it is convenient to reduce the two RMSE values to a single scalar number. We do this by defining the dimensionless metric Q_{init}:

$$Q_{\mathrm{init}} = \sqrt{\left(\frac{\mathrm{RMSE}(H)}{450\,\mathrm{m}}\right)^2 + \left(\frac{\mathrm{RMSE}(u)}{450\,\mathrm{m\,yr^{-1}}}\right)^2}. \tag{11}$$

The scaling values of 450 m and $450\,\mathrm{m\,yr^{-1}}$ for the ice thickness and velocity errors are chosen to bracket the ISMIP6 ensemble, so that a value of $Q_{\mathrm{init}} = 1$ implies a realisation that

Table 6. Parameter choices in the UFEMISM model ensemble.

Parameter	Options
Sliding law	Zoet–Iverson, Weertman ($m = 3$), Weertman ($m = 4$)
Bed roughness nudging scheme	H–u, H–dH/dt, H–dH/dt-local
Ocean forcing	WOA+quadratic, WOA-nudged+quadratic, inverted melt rates
Sub-grid melt scheme	FCMP, PMP
Grounding-line resolution	20, 10, 5, 3*, 2*, 1* km

* Only for Thwaites Glacier and Pine Island Glacier, 5 km everywhere else.

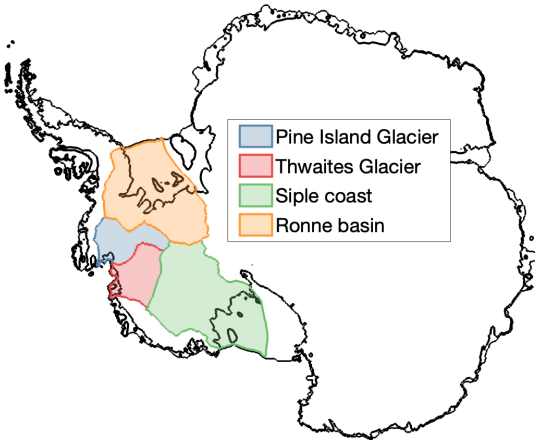

Figure 1. The IMBIE drainage basins of PIG (blue), TG (red), the Siple coast (green), and the Ronne ice shelf (orange).

is just slightly worse than the worst model in the ISMIP6 ensemble, whereas a value of $Q_{\text{init}} = 0$ implies a perfect match with both BedMachine and MEaSUREs.

While most of the currently observed mass loss occurs at PIG and TG, many models in the ISMIP6 ensemble also, or instead, project substantial grounding-line retreat and mass loss at the Siple coast, the Bungenstock ice rise, the Institute ice stream, and occasionally around the Millennium ice stream and the Totten ice shelf (Seroussi et al., 2024). In the UFEMISM realisations presented here (shown in Sect. 4), most of the mass loss is concentrated around the Siple coast, with secondary contributions from the Bungenstock ice rise and the western section of the Ronne ice shelf. We will therefore analyse our model results over the entire ice sheet, as well as over the individual drainage basins of PIG and TG, the Ronne ice shelf and basin, and the Siple coast area (using the IMBIE basins; Zwally et al., 2012; see Fig. 1).

4 Results

4.1 Initial states

Figure 2 shows RMSE(H) and RMSE(u) for all UFEMISM initialisations, compared to the models of the ISMIP6 ensemble by Seroussi et al. (2024, their Fig. 2, here recalculated for all model submissions). The different panels show these quantities calculated for the entire Antarctic ice sheet, as well as for the individual drainage basins.

In terms of ice thickness, the UFEMISM ensemble performs well relative to the ISMIP6 ensemble, with the pan-Antarctic RMSE varying from approximately 50 to 200 m (compared to about 60 to 360 m for the ISMIP6 ensemble – a larger range than reported by Seroussi et al. (2024), as they only reported each model's main submission). The velocity errors vary more widely, ranging from 70 to 390 m yr^{-1} (45 to 370 m yr^{-1} for the ISMIP6 ensemble). In the PIG, TG, and Ronne basins, most UFEMISM realisations and ISMIP6 models perform slightly worse than the pan-Antarctic average. Over PIG and TG, UFEMISM generally performs slightly better than the ISMIP6 ensemble, while over the Ronne basin, UFEMSIM produces comparable thickness errors but worse velocities. In the Siple coast area (a challenging region for models due to the presence of the relatively recently stagnated Kamb ice stream, causing a notable ice thickening rate), the UFEMISM realisations generally have small thickness errors, while the velocity errors show more variation though are still smaller than the pan-Antarctic average.

The values of the Q_{init} for the different drainage basins are compared to each other in Fig. 3. The ISMIP6 ensemble has values of $Q_{\text{init,pan}} \in [0.16, 0.9]$, whereas the UFEMISM ensemble has values of $Q_{\text{init,pan}} \in [0.26, 0.81]$. The pan-Antarctic and basin-specific values of Q_{init} are only weakly correlated, implying that the fact that a model produces a "good" match over the entire ice sheet is no guarantee that it performs comparably well in a particular drainage basin.

Figure 4 shows the errors in the modelled ice thickness and ice velocity, as well as the inverted bed roughness field, for the "best" UFEMISM simulation (i.e. with the lowest pan-Antarctic Q_{init}; see Fig. 2). This simulation used the Weertman ($m = 3$) sliding law, the H–u nudging method, the inverted basal melt rates, the FCMP sub-grid melt scheme, and a 1 km grounding-line resolution. The ice thickness is generally within 300 m of the observations. The largest errors in the ice velocity occur over the Pine Island and Thwaites shelves, with the former flowing too slowly in the center and too fast in the shear margins. For the Thwaites shelf, there is a clear asymmetry, with the eastern part flowing too

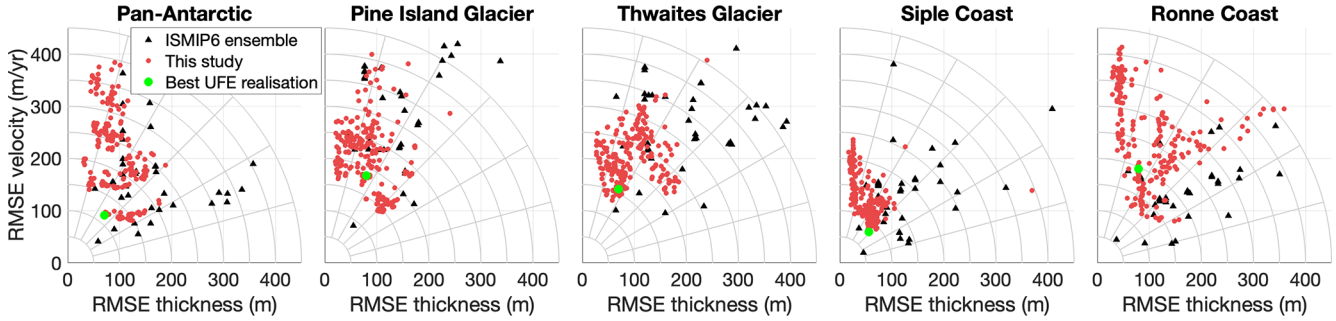

Figure 2. Red circles: errors with respect to observations of ice thickness (BedMachine Antarctica v3; Morlighem et al., 2017) and ice velocity (MEaSUREs Antarctica v2; Rignot et al., 2011) for the UFEMISM realisations; black triangles: the same for the models in the ISMIP6 ensemble (Seroussi et al., 2024, their Fig. 2). Green circle: the "best" UFEMISM realisation (i.e. with the lowest pan-Antarctic Q_{init}). The radial grid illustrates contours of equal Q_{init}.

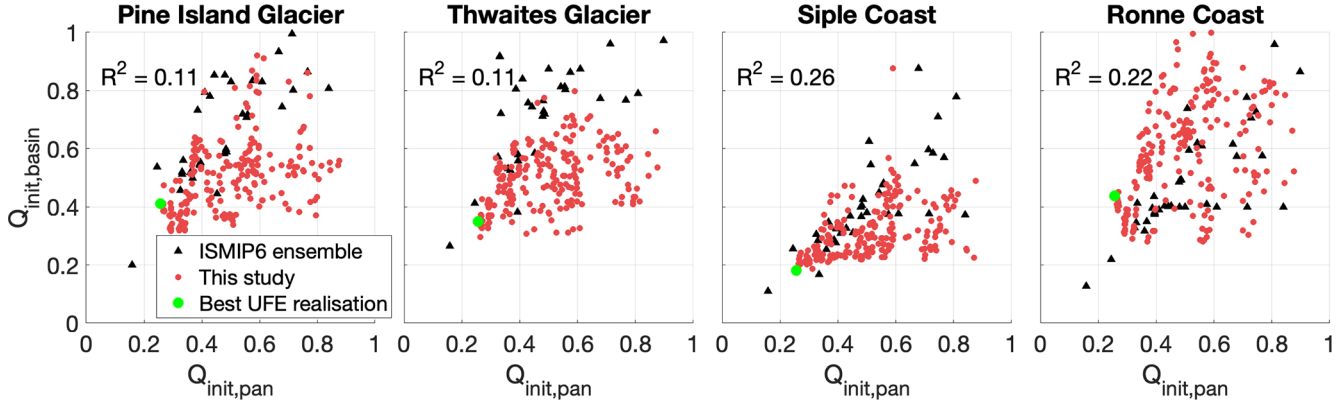

Figure 3. Comparison of the "quality of initial state" metric Q_{init} calculated for the entire Antarctic ice sheet ($Q_{\mathrm{init,pan}}$), versus for the individual drainage basins. The correlation coefficients R^2 are calculated only for the UFEMISM realisations, not for the ISMIP6 ensemble. The "best" UFEMISM realisation (green circle) is still the one with the lowest $Q_{\mathrm{init,pan}}$.

fast and the western part flowing too slowly. This might be a consequence of the absence of any damage modelling in UFEMISM (e.g. Bett et al., 2026). The inverted bed roughness field appears to be quite smooth; although we must stress that, since there are virtually no observations of the friction field, any judgment of such an inverted product is entirely subjective, it does suggest that the quality of our initial state does not result from overfitting.

Figure 5 shows how the choice of model parameters affects the pan-Antarctic thickness and velocity errors. As can be seen, the choice of sliding law and nudging method have the strongest influence on the ability of the model to produce an initial state close to the observations. For each of the three sliding laws, there are two "clusters" of model realisations, which differ in the choice of nudging scheme; the H–u scheme generally produces smaller errors in the ice velocity and larger errors in the ice thickness, while the H–$\mathrm{d}H/\mathrm{d}t$ scheme does the opposite. This seems logical, as the H–u scheme includes the errors with respect to the velocity observations in the calculation of the nudging weights. The reason for the different performance of the different sliding laws is less obvious, as allowing a free choice of friction coefficient means any sliding law should be able to produce the same distribution of basal shear stress. We suspect that the explanation involves the units of the bed friction coefficient, which can differ by several orders of magnitude between different sliding laws. While Eqs. (3) and (5) theoretically assume the friction coefficient C to be dimensionless, these differing magnitudes might affect the performance of the nudging scheme. Implementing dimensionless sliding laws along the lines of Greve (2025) might help solve these issues in future work. However, since the worst-performing UFEMISM realisations (combining the Zoet–Iverson sliding law and the H–$\mathrm{d}H/\mathrm{d}t$ nudging scheme) are still bracketed by the ISMIP6 ensemble, we do not deem this a critical issue at present.

The choice of ocean forcing has a small effect on the errors in the ice thickness, with the WOA+quadratic, WOA−nudged+quadratic, and inverted-BMB producing progressively smaller errors. Calculating the RMSE only over the ice shelves (not shown) results in a stronger effect of the choice of ocean forcing, since both the WOA−nudged+quadratic, and inverted-BMB options gen-

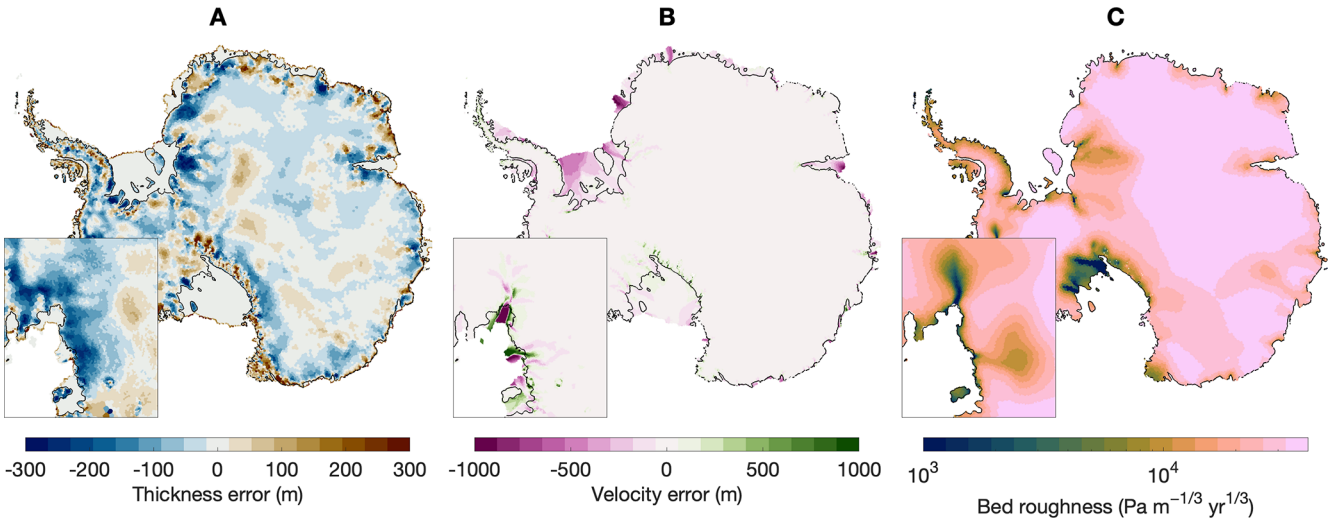

Figure 4. **(A)** Error in modelled ice thickness, **(B)** error in ice velocity, and **(C)** inverted bed roughness for the "best" UFEMISM simulation. Inset panels zoom in on the PIG and TG drainage basins.

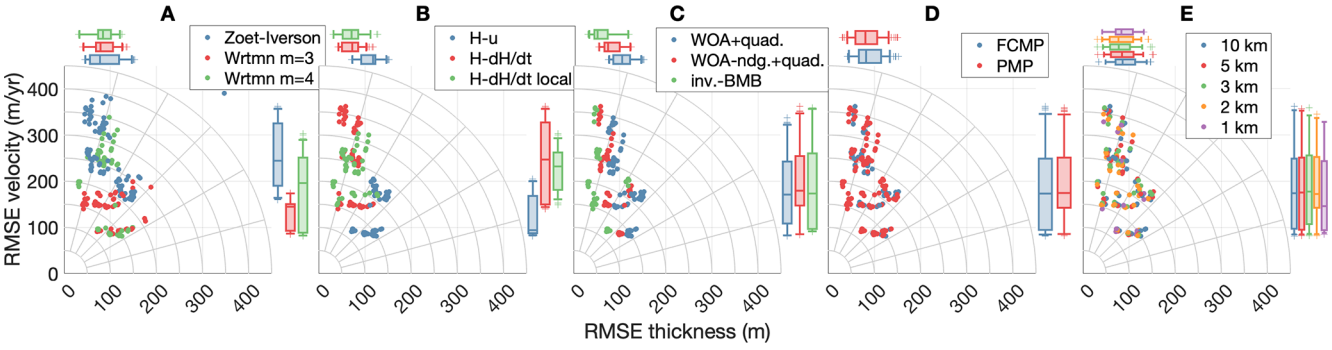

Figure 5. Errors with respect to observations of ice thickness (BedMachine Antarctica v3; Morlighem et al., 2017) and ice velocity (MEaSUREs Antarctica v2; Rignot et al., 2011) for all 180 UFEMISM realisations, as a function of the choice of model parameters: **(A)** sliding law, **(B)** nudging method, **(C)** ocean forcing, **(D)** sub-grid melt scheme, **(E)** grounding-line resolution. Box plots to the top and right of each panel show the distribution of RMSE's in respectively the ice thickness and velocity, for the different parameter choices. The radial grid illustrates contours of equal Q_{init}.

erally result in near-perfect shelves. The choices of sub-grid melt parameterisation and grounding-line resolution do not appear to have any significant effect on the agreement between model and observations.

4.2 Future projections

The sea level curves for all projections are shown in Fig. 6. The inset panel shows that the modelled sea-level rate in 2014 generally matches the observed rate of 0.41 mm yr^{-1}, indicating that the "thinning rate compensation during initialisation" approach by van den Akker et al. (2025) works well. However, whereas they find that their model continues that trend, and eventually sharply accelerates when the TG and/or PIG start to collapse, all UFEMISM projections stabilise within a few decades. It is only well into the 22nd century that some of the projections start to show an accelerating sea-level rate, although even then, the majority remain very stable. By the year 2300, that small cluster of simulations projects a SLC of 0.45–1.45 m; the larger cluster of "stable" simulations project between $\sim$ 35 cm of sea-level rise, and $\sim$ 12 cm of sea-level drop.

The general pattern of relatively little mass loss until 2100, a marked acceleration over the course of the 22nd century, and an approximately linear trend after 2200, is seen both in our results and in the majority of simulations in the ISMIP6 ensemble by Seroussi et al. (2024). That ensemble ranges between approximately -25 and $+25$ cm of sea-level contribution in 2100, completely enveloping the range of our results. The deceleration of the present-day sea-level trend in our results is likewise produced by a sizeable minority of the model realisations in the ISMIP6 ensemble. While the exact mechanism(s) responsible for the decelerating mass loss in

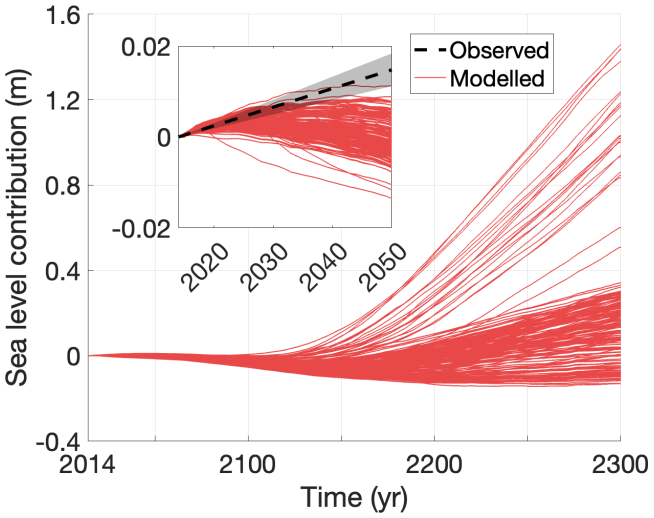

Figure 6. Projected SLC under SSP5-8.5 for the UFEMISM ensemble. The small inset panel shows the first 50 years, and includes the observed present-day Antarctic sea-level contribution rate of 0.41 mm yr^{-1}.

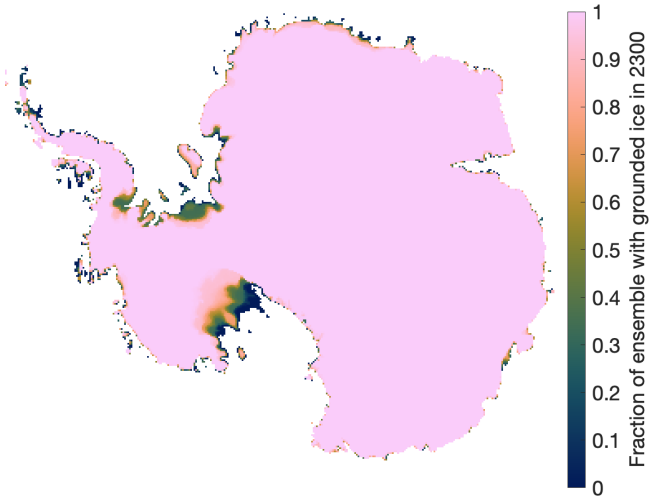

Figure 7. Fraction of models in the UFEMISM ensemble where currently grounded ice is still grounded in 2300.

the Amundsen Sea area in some ice-sheet models is not clear, and would be an interesting avenue for further research, we do not think it is central to our study (as we explicitly do not interpret out simulations as actual future projections).

Figure 7 shows where the mass loss occurs in the UFEMISM ensemble. Most of this is in the Siple coast area, with smaller contributions around the Bungenstock ice rise and the ice streams feeding into the western section of the Ronne ice shelf. The UFEMISM ensemble never shows any significant retreat of PIG and TG. The ISMIP6 ensemble is quite variable in this area, with a median retreat of the TG grounding line of about 100 km, and about 20 %–30 % of the ensemble showing no significant retreat at all (Seroussi et al., 2024, their Fig. 7). By contrast, over 90 % of models in the ISMIP6 ensemble project substantial mass loss and grounding-line retreat around the Bungenstock ice rise and the Siple coast, agreeing well with the UFEMISM ensemble presented here.

Figure 8 shows how the choice of model parameters affects the projected SLC. As with the initial states, the strongest effects are from the choice of sliding law and of the nudging method. The choice of ocean forcing, sub-grid melt parameterisation, and grounding-line resolution do not seem to have much effect on the projected SLC. The "cluster" of high-SLC realisations are those that combined the Zoet–Iverson sliding law with the H–u nudging method. All realisations using the Weertman sliding law (with both values of the exponent m) and/or the (local) H–$\mathrm{d}H/\mathrm{d}t$ nudging method lie within the low-SLC cluster.

Figure 9 shows the projected SLC under SSP5-8.5 as a function of the initial state quality metric Q_{init} for the entire Antarctic ice sheet, as well as for the individual drainage basins. The small cluster of high-SLC realisations is clearly visible. These simulations all have their pan-Antarctic values of Q_{init} clustered between values of 0.5–0.6, while for the individual drainage basins, the quality of their initial states is more variable. Whether looking at the entire Antarctic ice sheet, or considering any specific basins, there appears to be no relation between the quality of a model's initial state, and the SLC it projects in the future.

We additionally used our ensemble of initial states to perform the ABUMIP-ABUK experiment (Sun et al., 2020), where the ice sheet is subjected to the instantaneous and sustained removal of all ice shelves. While this forcing is extreme bordering on the unphysical, it serves as a useful end-member. The resulting sea-level curves as a function of the model choices, similar to Fig. 8, are shown in Appendix A. The general pattern of the variance in SLC is the same as for the SSP5-8.5 results in Fig. 8, being dominated by the choices of sliding law and nudging scheme, with negligible contributions from the ocean forcing, the sub-grid melt scheme, and the resolution.

5 Discussion and conclusion

We have presented an ensemble of realisations of the Antarctic ice sheet with the UFEMISM ice-sheet model. These realisations differ by several model parameter choices, including the sliding law, the sub-shelf melt forcing, and numerical parameters such as the algorithm used to invert for the bed roughness, the choice of sub-grid melt parameterisation at the grounding line, and the grid resolution. We have shown that, for all combinations of parameter choices, inverting for the bed roughness can produce a steady-state ice sheet that matches satellite-derived observations of the ice surface elevation and velocity, to the same degree as the recent ISMIP6

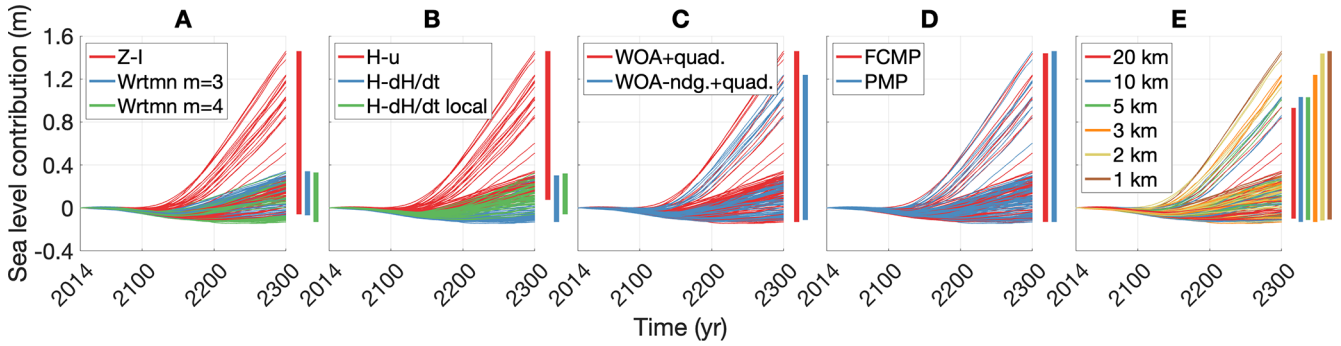

Figure 8. Projected SLC under SSP5-8.5 for the UFEMISM ensemble, showing the effects of the different model parameters. **(A)** Sliding laws: Zoet–Iverson (blue), Weertman with $m = 3$ (red), Weertman with $m = 4$ (red). **(B)** Nudging methods: H–u (blue), H–dH/dt (red), H–dH/dt local (green). **(C)** Ocean forcing: WOA with quadratic melt parameterisation (blue), WOA with nudged temperatures with quadratic melt parameterisation (red). **(D)** sub-grid melt parameterisations: FCMP (blue), PMP (red). **(E)** grounding-line resolutions: 10 km (blue), 5 km (red), 3 km (green), 2 km (orange), 1 km (purple). Coloured bars on the right-hand side of each graph show the range of projected SLC in the year 2300 for each parameter choice.

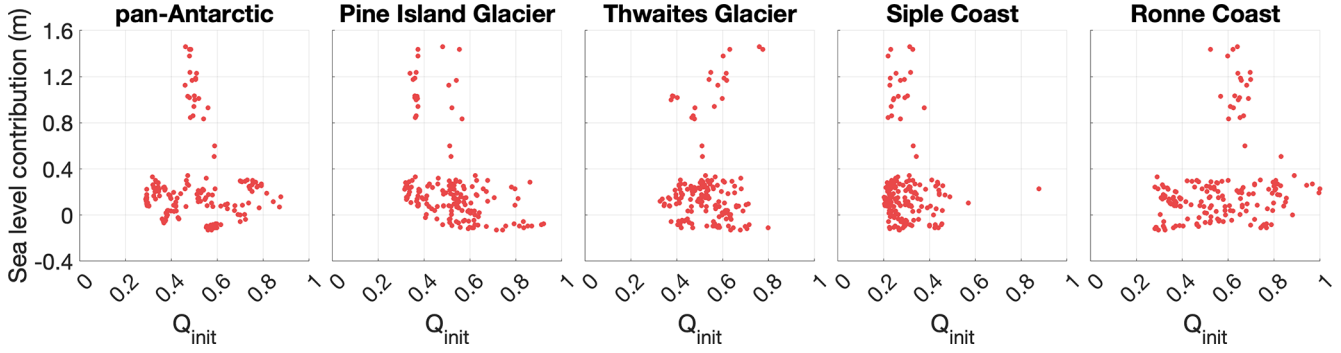

Figure 9. projected SLC under SSP5-8.5 as a function of the initial state quality metric Q_{init}, calculated for **(A)** the entire Antarctic ice sheet, as well as only for **(B)** the PIG and **(C)** the TG drainage basins.

model ensemble (Seroussi et al., 2024). When projected into the future under the high-warming SSP5-8.5 scenario, these model realisations differ strongly in their projected sea-level contribution, varying from approximately 30 cm of sea-level drop to up to 1.5 m of sea-level rise in 2300. This is a lower limit to the 'real' uncertainty, as the selection of parameters that were varied in our ensemble is by no means exhaustive. For example, processes involving subglacial hydrology, ice fabric, damage, and calving are all highly parameterised or outright neglected in our model set-up. The biases that these missing processes introduce into the present-day ice-sheet geometry and velocity are compensated for by the inversions for basal friction and sub-shelf melt, all of which can bias the response of the ice sheet to climate forcing. Additionally sampling the uncertainty in these processes would increase the variance in the projected SLC even further.

In our ensemble, this variance is dominated by the choice of sliding law and of the algorithm used to invert for the bed roughness. Those two model choices also have the strongest effect on the "quality" of the model's initial state, following the ISMIP6 approach of defining this as the RMSE between the modelled and satellite-derived ice surface elevation and velocity. However, there appears to be no relation between the quality of the initial state of a model, and the amount of SLC it projects, regardless of whether that quality is assessed for the entire Antarctic ice sheet, or for only the PIG and/or TG basins. In recent years, there has been discussion amongst the ice-sheet modelling community about the large differences between the "quality" of the initial states of different models in the ISMIP ensembles. While previous studies within ISMIP have always opted to allow all model submissions regardless of the quality of their initial state, it has been proposed that future model ensembles should exclude models that fail to meet a certain minimum quality (with subsequent discussions about how that quality should be quantified), or as a compromise, that individual models should be weighted by their initial state quality when performing statistical analysis of the ensemble (mean, median, etc.). However, our UFEMISM realisations show no relation between the quality of the initial states, and the projected SLC. Weighting or even excluding individual simulations would therefore not strongly affect the ensemble statistics.

There have also been suggestions to judge models based on how well they reproduce the observed mass loss trend, either in terms of the spatial pattern (along the lines of Goldberg and Holland, 2022, or van den Akker et al., 2025), or in terms of in the integrated mass loss, i.e., the contribution to sea-level rise (along the lines of Otosaka et al., 2023). However, when compared to the existing uncertainties in ice-sheet models, the present-day mass loss trends are small. Extrapolating Antarctica's present-day sea-level contribution of about 0.4 mm yr^{-1} produces just over 10 cm of sea-level rise in 2300, a signal that vanishes beneath the uncertainty from the applied climate forcing and other uncertainties. Similarly, van den Akker et al. (2025) find that the acceleration away from the present-day trend, and the resulting committed collapse of the Amundsen Sea basin, in most of their simulations only initiates after 2300. These findings suggest that the bias that is introduced by not including the present-day trend, is obscured by the many other existing uncertainties in ice-sheet models.

The satellite-derived observations of the ice-sheet surface elevation and velocity that are used a priori as "targets" for the initial state of the ice-sheet model, and a posteriori to assess the quality of the initial state, all carry their own uncertainties. Adjoint-based inversion methods often include this observational uncertainty in the cost function, assigning less weight to errors in locations where the observations are less certain. Introducing a similar weighting into our nudging scheme could be an interesting avenue for future work. However, aside from uncertainties, the observational datasets also can carry biases. Most ice-sheet models in the ISMIP6 ensemble, including UFEMISM, treat these data as 'snapshots' of the ice sheet at a certain fixed point in time. However, since the satellites do not pass over every location on the ice sheet every day, and because weather conditions do not always permit clear observations of the surface, datasets such as BedMachine and MEaSUREs are, in fact, aggregates of several years of observations, with irregular spatial and temporal coverage that differs between the datasets. There can be significant variations in both the ice geometry (mostly over the shelves, parts of which may have calved between years) and the ice velocity between those years, leading to inconsistencies in the aggregated dataset. For example, ice velocities in the MEaSUREs dataset over the TG basin can vary by over 15 % on a year-to-year basis, even hundreds of kilometres upstream of the grounding line. Superimposed on the annual variations is an accelerating trend, caused by the incrementally collapsing shelf and the subsequent retreat of the grounding line. Since the different datasets have a different temporal coverage, this implies that it might not be possible for a numerical model to perfectly reproduce both the observed geometry and velocity simultaneously – or that, if it does, it might well be for the wrong reasons.

Our results show that the choice of sliding law strongly affects the projected SLC, similar to findings by earlier studies (e.g. Sun et al., 2020). When using only "snapshot" observations of the ice surface, it is fundamentally impossible to derive both the form of the sliding law and the bed roughness at the same time, as the instantaneous velocity distribution follows from the distribution of the basal shear stress, which can arise from any sliding law, given the proper distribution of bed roughness. Aside from theoretical considerations and laboratory experiments, the sliding law can only be derived from empirical observations if temporal variations are included. For example, Trevers et al. (2024) used temporal observations of Jakobshavn Isbrae in Greenland to conclude that an ice-sheet model with a regularised Coulomb sliding law was best able to reproduce those observations. Applying similar methods to PIG and TG to determine the sliding laws governing those ice sheets could prove valuable, though complicated, as the temporal variations in velocity there are linked to variations in buttressing due to both calving and damage of the shelves – processes that are poorly or not at all represented in many ice-sheet models. Furthermore, the basal shear stress applied by the substrate to the sliding base of the ice is modulated by the presence of liquid water between the ice and the substrate. This subglacial hydrological system is yet another component of the ice-sheet system that is poorly understood, and consequently poorly or not at all represented in many ice-sheet models. Recent studies have shown that adding such processes to a model can strongly affect its response to climate forcing (e.g. Kazmierczak et al., 2022).

The misrepresentation or absence of physical processes such as calving, damage, and subglacial hydrology leads to biases in ice-sheet models. However, when inverse methods such as the nudging schemes discussed here are used to derive the distribution of bed roughness or basal shear stress, those biases are (partially or mostly) compensated for by opposite errors in the bed roughness. Berends et al. (2023b) showed that such compensating errors imply that the initial state of the model might look "correct", but for the wrong reasons – and that the SLC that is found when integrating that model into the future is still affected. This implies that using the "quality" of a model's initial state to weight or even exclude it from a model ensemble might not achieve the desired result of producing a more reliable ensemble, as this could potentially exclude models that have "better" physics forced with imperfect input, in favour of models with "worse" physics, where the resulting errors are erroneously compensated for by an inversion. Only if and when more, and more reliable observations of the ice-sheet's sub-surface and temporal evolution become available, and more robust methods are developed to assess a model's ability to reproduce them, will we be able to further reduce the range of possible parameter choices, and thereby the uncertainty in future projections of Antarctica's SLC.

Appendix A: ABUMIP

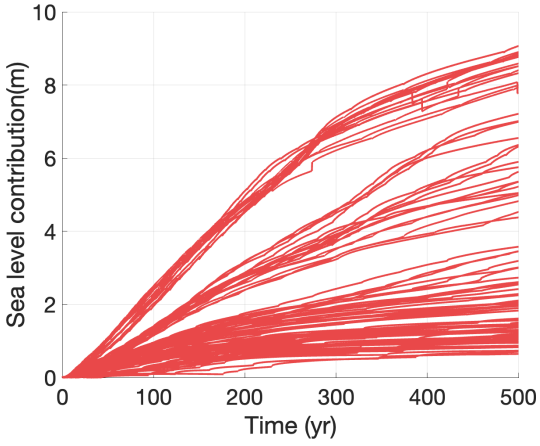

Figure A1. Projected SLC in the ABUMIP-ABUK experiment for the UFEMISM ensemble.

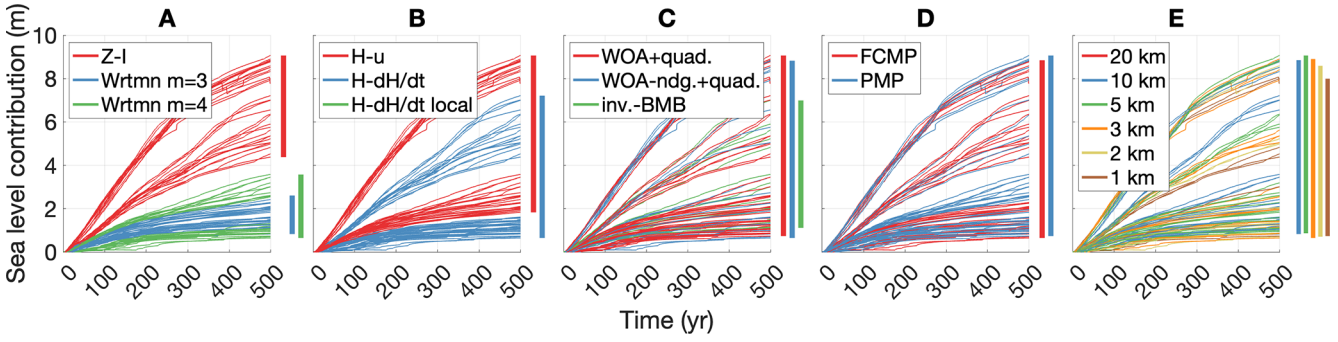

Figure A2. Projected SLC in the ABUMIP-ABUK experiment, showing the effects of the different model parameters. **(A)** Sliding laws: Zoet-Iverson (blue), Weertman with $m = 3$ (red), Weertman with $m = 4$ (red). **(B)** Nudging methods: H–u (blue), H–dH/dt (red), H–dH/dt local (green). **(C)** Ocean forcing: WOA with quadratic melt parameterisation (blue), WOA with nudged temperatures with quadratic melt parameterisation (red). **(D)** Sub-grid melt parameterisations: FCMP (blue), PMP (red). **(E)** Grounding-line resolutions: 10 km (blue), 5 km (red), 3 km (green), 2 km (orange), 1 km (purple). Coloured bars on the right-hand side of each graph show the range of projected SLC after 500 years for each parameter choice.

To assess the response of the different UFEMISM realisations to an extreme high-end forcing, and verify that the model can in principle produce a collapse of the entire West Antarctic ice sheet from ice dynamics alone, we also performed the instantaneous-collapse ABUK experiment from the Antarctic Buttressing Model Intercomparison Project (ABUMIP; Sun et al., 2020), where all floating ice is removed during the simulation. The surface mass balance is kept unchanged from the initialisation during these simulations, so that no mass loss from climate change is included; any mass loss is caused by the complete loss of buttressing, which can, depending on model choices, result in a complete collapse of the West Antarctic ice sheet, and in substantial retreat in several marine-grounded sectors of East Antarctica. The sea-level curves of the different UFEMISM simulations are shown in Fig. A1. The sea-level contribution at the end of the 500-year experiment varies from 0.6 to 9.1 m, comparing well to the range of 2–10 m of the multi-model ensemble in Sun et al. (2020). Note that this ensemble also includes projections from the "inverted melt rates" initial states; since no shelves exist in the projections, the difficulty of extrapolating the inverted melt rates is negated.

Figure A2 shows how the choice of model parameters affects the projected SLC. As in the SSP5-8.5 simulations, the strongest effects are from the choice of sliding law and the nudging method. The sub-shelf melt forcing, sub-grid melt parameterisation, and model resolution do not seem to be very important.

Code and data availability. The exact version of the UFEMISM2.0 source code that was used to produce the results presented here is available at https://doi.org/10.5281/zenodo.8434468 (Berends et al., 2026).

Author contributions. All authors contributed to defining the research topic. CJB, JAB and EL wrote the model code. CJB performed the experiments, analysed the results, and wrote the first draft of the manuscript. All authors contributed to the final manuscript.

Competing interests. The contact author has declared that none of the authors has any competing interests.

Disclaimer. Publisher's note: Copernicus Publications remains neutral with regard to jurisdictional claims made in the text, published maps, institutional affiliations, or any other geographical representation in this paper. The authors bear the ultimate responsibility for providing appropriate place names. Views expressed in the text are those of the authors and do not necessarily reflect the views of the publisher.

Acknowledgements. We thank the ISMIP community for discussing the topic of this study with us, and particularly Bill Lipscomb, Gunter Leguy, and Tim van den Akker for discussing some of our preliminary results. We also thank Tim van den Akker for sharing the technical details of the new bed roughness nudging scheme in CISM, Samuel Cook for his work as editor, and two anynomous reviewers for providing constructive criticism on the manuscript.

Financial support. CJB and JAB have been supported by the Nederlandse Organisatie voor Wetenschappelijk Onderzoek (NWO), Exacte en Natuurwetenschappen (grant no. OCENW.KLEIN.515). Erwin Lambert was funded by the Knowledge Programme Sea Level Rise, which received funding from the Dutch Ministry of Infrastructure and Water Management.

Review statement. This paper was edited by Samuel Cook and reviewed by two anonymous referees.

References

Arthern, R. J. and Gudmundsson, G. H.: Initialization of ice-sheet forecasts viewed as an inverse Robin problem, J. Glaciol., 56, 527–533, 2010.

Arthern, R. J., Hindmarsh, R. C. A., and Williams, C. R.: Flow speed within the Antarctic ice sheet and its controls inferred from satellite observations, J. Geophys. Res.-Earth, 120, 1171–1188, 2015.

Asay-Davis, X. S., Cornford, S. L., Durand, G., Galton-Fenzi, B. K., Gladstone, R. M., Gudmundsson, G. H., Hattermann, T., Holland, D. M., Holland, D., Holland, P. R., Martin, D. F., Mathiot, P., Pattyn, F., and Seroussi, H.: Experimental design for three interrelated marine ice sheet and ocean model intercomparison projects: MISMIP v. 3 (MISMIP +), ISOMIP v. 2 (ISOMIP +) and MISOMIP v. 1 (MISOMIP1), Geosci. Model Dev., 9, 2471–2497, https://doi.org/10.5194/gmd-9-2471-2016, 2016.

Berends, C. J., Stap, L. B., and van de Wal, R. S. W.: Strong impact of sub-shelf melt parameterisation on ice-sheet retreat in idealised and realistic Antarctic topography, J. Glaciol., 69, 1434–1448, https://doi.org/10.1017/jog.2023.33, 2023a.

Berends, C. J., van de Wal, R. S. W., van den Akker, T., and Lipscomb, W. H.: Compensating errors in inversions for subglacial bed roughness: same steady state, different dynamic response, The Cryosphere, 17, 1585–1600, https://doi.org/10.5194/tc-17-1585-2023, 2023b.

Berends, C. J., Azizi, V., Bernales, J. A., and van de Wal, R. S. W.: The Utrecht Finite Volume Ice-Sheet Model (UFEMISM) version 2.0 – Part 1: Description and idealised experiments, Geosci. Model Dev., 18, 3635–3659, https://doi.org/10.5194/gmd-18-3635-2025, 2025.

Berends, T., Bernales, J., Azizi, V., and van de Wal, R.: UFEMISM2.0, Zenodo [computer software], https://doi.org/10.5281/zenodo.8434468, 2026.

Bett, D. T., Bradley, A. T., Miles, B. W. J., Williams, C. R., Holland, P. R., and Arthern, R. J.: Modelling the evolution of Thwaites Glacier over the 20th century, EGUsphere [preprint], https://doi.org/10.5194/egusphere-2026-669, 2026.

Burgard, C., Jourdain, N. C., Reese, R., Jenkins, A., and Mathiot, P.: An assessment of basal melt parameterisations for Antarctic ice shelves, The Cryosphere, 16, 4931–4975, https://doi.org/10.5194/tc-16-4931-2022, 2022.

Castleman, B. A., Schlegel, N.-J., Caron, L., Larour, E., and Khazendar, A.: Derivation of bedrock topography measurement requirements for the reduction of uncertainty in ice-sheet model projections of Thwaites Glacier, The Cryosphere, 16, 761–778, https://doi.org/10.5194/tc-16-761-2022, 2022.

Cheng, G., Lötstedt, P., and von Sydow, L.: Accurate and stable time stepping in ice sheet modeling, J. Comput. Phys., 329, 29–47, 2017.

Cornford, S. L., Seroussi, H., Asay-Davis, X. S., Gudmundsson, G. H., Arthern, R., Borstad, C., Christmann, J., Dias dos Santos, T., Feldmann, J., Goldberg, D., Hoffman, M. J., Humbert, A., Kleiner, T., Leguy, G., Lipscomb, W. H., Merino, N., Durand, G., Morlighem, M., Pollard, D., Rückamp, M., Williams, C. R., and Yu, H.: Results of the third Marine Ice Sheet Model Intercomparison Project (MISMIP+), The Cryosphere, 14, 2283–2301, https://doi.org/10.5194/tc-14-2283-2020, 2020.

Coulon, V., Klose, A. K., Kittel, C., Edwards, T., Turner, F., Winkelmann, R., and Pattyn, F.: Disentangling the drivers of future Antarctic ice loss with a historically calibrated ice-sheet model, The Cryosphere, 18, 653–681, https://doi.org/10.5194/tc-18-653-2024, 2024.

Coulon, V., Klose, A. K., Edwards, T., Turner, F., Pattyn, F., and Winkelmann, R.: From short-term uncertainties to long-term certainties in the future evolution of the Antarctic Ice Sheet, Nat. Commun., 16, 10385, https://doi.org/10.1038/s41467-025-66178-w, 2025.

DeConto, R. M. and Pollard, D.: Contribution of Antarctica to past and future sea-level rise, Nature, 531, 591–597, 2016.

Favier, L., Jourdain, N. C., Jenkins, A., Merino, N., Durand, G., Gagliardini, O., Gillet-Chaulet, F., and Mathiot, P.: Assessment of sub-shelf melting parameterisations using the ocean–ice-sheet coupled model NEMO(v3.6)–Elmer/Ice(v8.3) , Geosci. Model Dev., 12, 2255–2283, https://doi.org/10.5194/gmd-12-2255-2019, 2019.

Gagliardini, O., Zwinger, T., Gillet-Chaulet, F., Durand, G., Favier, L., de Fleurian, B., Greve, R., Malinen, M., Martín, C., Råback, P., Ruokolainen, J., Sacchettini, M., Schäfer, M., Seddik, H., and Thies, J.: Capabilities and performance of Elmer/Ice, a new-generation ice sheet model, Geosci. Model Dev., 6, 1299–1318, https://doi.org/10.5194/gmd-6-1299-2013, 2013.

Getraer, B. and Morlighem, M.: Increasing the Glen–Nye Power-Law Exponent Accelerates Ice-Loss Projections for the Amundsen Sea Embayment, West Antarctica, Geophys. Res. Lett., 52, e2024GL112516, https://doi.org/10.1029/2024GL112516, 2025.

Goelzer, H., Nowicki, S., Edwards, T., Beckley, M., Abe-Ouchi, A., Aschwanden, A., Calov, R., Gagliardini, O., Gillet-Chaulet, F., Golledge, N. R., Gregory, J., Greve, R., Humbert, A., Huybrechts, P., Kennedy, J. H., Larour, E., Lipscomb, W. H., Le clec'h, S., Lee, V., Morlighem, M., Pattyn, F., Payne, A. J., Rodehacke, C., Rückamp, M., Saito, F., Schlegel, N., Seroussi, H., Shepherd, A., Sun, S., van de Wal, R., and Ziemen, F. A.: Design and results of the ice sheet model initialisation experiments initMIP-Greenland: an ISMIP6 intercomparison, The Cryosphere, 12, 1433–1460, https://doi.org/10.5194/tc-12-1433-2018, 2018.

Goldberg, D. N.: A variationally derived, depth-integrated approximation to a higher-order glaciological flow model, J. Glaciol., 57, 157–170, 2011.

Goldberg, D. N. and Holland, P. R.: The Relative Impacts of Initialization and Climate Forcing in Coupled Ice Sheet-Ocean Modeling: Application to Pope, Smith, and Kohler Glaciers, J. Geophys. Res.-Earth, 127, e2021JF006570, https://doi.org/10.1029/2021JF006570, 2022.

Greve, R.: On non-dimensional forms of basal sliding laws and flow laws for ice-sheet and glacier modelling, J. Glaciol., 71, e123, https://doi.org/10.1017/jog.2025.10100, 2025.

Gudmundsson, G. H. and Raymond, M.: On the limit to resolution and information on basal properties obtainable from surface data on ice streams, The Cryosphere, 2, 167–178, https://doi.org/10.5194/tc-2-167-2008, 2008.

Jourdain, N. C., Asay-Davis, X., Hattermann, T., Straneo, F., Seroussi, H., Little, C. M., and Nowicki, S.: A protocol for calculating basal melt rates in the ISMIP6 Antarctic ice sheet projections, The Cryosphere, 14, 3111–3134, https://doi.org/10.5194/tc-14-3111-2020, 2020.

Kazmierczak, E., Sun, S., Coulon, V., and Pattyn, F.: Subglacial hydrology modulates basal sliding response of the Antarctic ice sheet to climate forcing, The Cryosphere, 16, 4537–4552, https://doi.org/10.5194/tc-16-4537-2022, 2022.

Klose, A. K., Coulon, V., Pattyn, F., and Winkelmann, R.: The long-term sea-level commitment from Antarctica, The Cryosphere, 18, 4463–4492, https://doi.org/10.5194/tc-18-4463-2024, 2024.

Larour, E., Seroussi, H., Morlighem, M., and Rignot, E.: Continental scale, high order, high spatial resolution, ice sheet modeling using the Ice Sheet System Model (ISSM), J. Geophys. Res., 117, F01022, https://doi.org/10.1029/2011JF002140, 2012.

Lambert, E. and Burgard, C.: Brief communication: Sensitivity of Antarctic ice shelf melting to ocean warming across basal melt models, The Cryosphere, 19, 2495–2505, https://doi.org/10.5194/tc-19-2495-2025, 2025.

Lecavalier, B. S. and Tarasov, L.: A history-matching analysis of the Antarctic Ice Sheet since the Last Interglacial – Part 1: Ice sheet evolution, The Cryosphere, 19, 919–953, https://doi.org/10.5194/tc-19-919-2025, 2025.

Leguy, G. R., Lipscomb, W. H., and Asay-Davis, X. S.: Marine ice sheet experiments with the Community Ice Sheet Model, The Cryosphere, 15, 3229–3253, https://doi.org/10.5194/tc-15-3229-2021, 2021.

Lipscomb, W. H., Leguy, G. R., Jourdain, N. C., Asay-Davis, X., Seroussi, H., and Nowicki, S.: ISMIP6-based projections of ocean-forced Antarctic Ice Sheet evolution using the Community Ice Sheet Model, The Cryosphere, 15, 633–661, https://doi.org/10.5194/tc-15-633-2021, 2021.

Locarnini, R. A., Mishonov, A. V., Baranova, O. K., Boyer, T. P., Zweng, M. M., Garcia, H. E., Reagan, J. R., Seidov, D., Weathers, K. W., Paver, C. R., and Smolyar, I. V.: World Ocean Atlas 2018, Volume 1: Temperature, Tech. Rep. Atlas NESDIS 81, NOAA, https://data.nodc.noaa.gov/woa/WOA18/DOC/woa18_vol1.pdf (last access: 14 October 2025), 2019.

Morlighem, M., Williams, C. N., Rignot, E., An, L., Arndt, J. E., Bamber, J. L., Catania, G., Chauché, N., Dowdeswell, J. A., Dorschel, B., Fenty, I., Hogan, K., Howat, I., Hubbard, A., Jakobsson, M., Jordan, T. M., Kjeldsen, K. K., Millan, R., Mayer, L., Mouginot, J., Noël, B. P. Y., O'Cofaigh, C., Palmer, S., Rysgaard, S., Seroussi, H., Siegert, M. J., Slabon, P., Straneo, F., van den Broeke, M. R., Weinrebe, W., Wood, M., and Zinglersen, K. B.: BedMachine v3: Complete Bed Topography and Ocean Bathymetry Mapping of Greenland From Multibeam Echo Sounding Combined With Mass Conservation, Geophys. Res. Lett., 11051–11061, 2017.

Noël, B., van Wessem, J. M., Wouters, B., Trusel, L., Lhermitte, S., and van den Broeke, M. R.: Higher Antarctic ice sheet accumulation and surface melt rates revealed at 2 km resolution, Nature Communications 14, 7949, https://doi.org/10.1038/s41467-023-43584-6, 2023.

Otosaka, I. N., Shepherd, A., Ivins, E. R., Schlegel, N.-J., Amory, C., van den Broeke, M. R., Horwath, M., Joughin, I., King, M. D., Krinner, G., Nowicki, S., Payne, A. J., Rignot, E., Scambos, T., Simon, K. M., Smith, B. E., Sørensen, L. S., Velicogna, I., Whitehouse, P. L., A, G., Agosta, C., Ahlstrøm, A. P., Blazquez, A., Colgan, W., Engdahl, M. E., Fettweis, X., Forsberg, R., Gallée, H., Gardner, A., Gilbert, L., Gourmelen, N., Groh, A., Gunter, B. C., Harig, C., Helm, V., Khan, S. A., Kittel, C., Konrad, H., Langen, P. L., Lecavalier, B. S., Liang, C.-C., Loomis, B. D., McMillan, M., Melini, D., Mernild, S. H., Mottram, R., Mouginot, J., Nilsson, J., Noël, B., Pattle, M. E., Peltier, W. R., Pie, N., Roca, M., Sasgen, I., Save, H. V., Seo, K.-W., Scheuchl, B., Schrama, E. J. O., Schröder, L., Simonsen, S. B., Slater, T., Spada, G., Sutterley, T. C., Vishwakarma, B. D., van Wessem, J. M., Wiese, D., van der Wal, W., and Wouters, B.: Mass balance of the Greenland and Antarctic ice sheets from 1992 to 2020, Earth Syst. Sci. Data, 15, 1597–1616, https://doi.org/10.5194/essd-15-1597-2023, 2023.

Pollard, D. and DeConto, R. M.: A simple inverse method for the distribution of basal sliding coefficients under ice sheets, applied to Antarctica, The Cryosphere, 6, 953–971, https://doi.org/10.5194/tc-6-953-2012, 2012.

Rignot, E., Mouginot, J., and Scheuchl, B.: Ice Flow of the Antarctic Ice Sheet, Science, 333, 1427–1430, 2011.

Robinson, A., Alvarez-Solas, J., Montoya, M., Goelzer, H., Greve, R., and Ritz, C.: Description and validation of the ice-sheet model Yelmo (version 1.0), Geosci. Model Dev., 13, 2805–2823, https://doi.org/10.5194/gmd-13-2805-2020, 2020.

Schoof, C.: The effect of cavitation on glacier sliding, P. R. Soc. A, 461, 609–627, 2005.

Seroussi, H., Nowicki, S., Simon, E., Abe-Ouchi, A., Albrecht, T., Brondex, J., Cornford, S., Dumas, C., Gillet-Chaulet, F., Goelzer, H., Golledge, N. R., Gregory, J. M., Greve, R., Hoffman, M. J., Humbert, A., Huybrechts, P., Kleiner, T., Larour, E., Leguy, G., Lipscomb, W. H., Lowry, D., Mengel, M., Morlighem, M., Pattyn, F., Payne, A. J., Pollard, D., Price, S. F., Quiquet, A., Reerink, T. J., Reese, R., Rodehacke, C. B., Schlegel, N.-J., Shepherd, A., Sun, S., Sutter, J., Van Breedam, J., van de Wal, R. S. W., Winkelmann, R., and Zhang, T.: initMIP-Antarctica: an ice sheet model initialization experiment of ISMIP6, The Cryosphere, 13, 1441–1471, https://doi.org/10.5194/tc-13-1441-2019, 2019.

Seroussi, H., Pelle, T., Lipscomb, W. H., Abe-Ouchi, A., Albrecht, T., Alvarez-Solas, J., Asay-Davis, X., Barre, J.-B., Berends, C. J., Bernales, J., Blasco, J., Caillet, J., Chandler, D. M., Coulon, V., Cullather, R., Dumas, C., Galton-Fenzi, B. K., Garbe, J., Gillet-Chaulet, F., Gladstone, R., Goelzer, H., Golledge, N., Greve, R., Gudmundsson, G. H., Han, H. K., Hillebrand, T. R., Hoffman, M. J., Huybrechts, P., Jourdain, N. C., Klose, A. K., Langebroek, P. M., Leguy, G. R., Lowry, D. P., Mathiot, P., Montoya, M., Morlighem, M., Nowicki, S., Pattyn, F., Payne, A. J., Quiquet, A., Reese, R., Robinson, A., Saraste, L., Simon, E. G., Sun, S., Twarog, J. P., Trusel, L. D., Urruty, B., Van Breedam, J., van de Wal, R. S. W., Wang, Y., Zhao, C., and Zwinger, T.: Evolution of the Antarctic Ice Sheet Over the Next Three Centuries From an ISMIP6 Model Ensemble, Earth's Future 12, e2024EF004561, https://doi.org/10.1029/2024EF004561, 2024.

Smith, B., Fricker, H. A., Gardner, A. S., Medley, B., Nilsson, J., Paolo, F. S., Holschuh, N., Adusumilli, S., Brunt, K., Csatho, B., Harbeck, K., Markus, T., Neumann, T., Siegfried, M. R., and Zwally, H. J.: Pervasive ice sheet mass loss reflects competing ocean and atmosphere processes, Science, 368, 1239–1242, 2020.

Sun, S., Pattyn, F., Simon, E. G., Albrecht, T., Cornford, S., Calov, R., Dumas, C., Gillet-Chaulet, F., Goelzer, H., Golledge, N. R., Greve, R., Hoffman, M. J., Humbert, A., Kazmierczak, E., Kleiner, T., Leguy, G. R., Lipscomb, W. H., Martin, D., Morlighem, M., Nowicki, S., Pollard, D., Price, S., Quiquet, A., Seroussi, H., Schlemm, T., Sutter, J., van de Wal, R. S. W., Winkelmann, R., and Zhang, T.: Antarctic ice sheet response to sudden and sustained ice-shelf collapse (ABUMIP), J. Glaciol., 66, 891–904, 2020.

Trevers, M., Payne, A. J., and Cornford, S. L.: Application of a regularised Coulomb sliding law to Jakobshavn Isbræ, western Greenland, The Cryosphere, 18, 5101–5115, https://doi.org/10.5194/tc-18-5101-2024, 2024.

Tsai, V. C., Stewart, A. L., and Thompson, A. F.: Marine ice-sheet profiles and stability under Coulomb basal conditions, J. Glaciol., 61, 205–215, 2015.

van den Akker, T., Lipscomb, W. H., Leguy, G. R., Bernales, J., Berends, C. J., van de Berg, W. J., and van de Wal, R. S. W.: Present-day mass loss rates are a precursor for West Antarctic Ice Sheet collapse, The Cryosphere, 19, 283–301, https://doi.org/10.5194/tc-19-283-2025, 2025.

van de Wal, R. S. W., Nicholls, R. J., Behar, D., McInnes, K., Stammer, D., Lowe, J. A., Church, J. A., DeConto, R., Fettweis, X., Goelzer, H., Haasnoot, M., Haigh, I. D., Hinkel, J., Horton, B. P., James, T. S., Jenkins, A., LeCozannet, G., Levermann, A., Lipscomb, W. H., Marzeion, B., Pattyn, F., Payne, A. J., Pfeffer, W. T., Price, S. F., Seroussi, H., Sun, S., Veatch, W., and White, K.: A High-End Estimate of Sea Level Rise for Practitioners, Earth's Future, 10, e2022EF002751, https://doi.org/10.1029/2022EF002751, 2022.

van Pelt, W. J. J., Oerlemans, J., Reijmer, C. H., Pettersson, R., Pohjola, V. A., Isaksson, E., and Divine, D.: An iterative inverse method to estimate basal topography and initialize ice flow models, The Cryosphere, 7, 987–1006, https://doi.org/10.5194/tc-7-987-2013, 2013.

Weertman, J.: On the sliding of glaciers, J. Glaciol., 3, 33–38, 1957.

Weertman, J.: Stability of the Junction of an Ice Sheet and an Ice Shelf, J. Glaciol., 13, 3–11, 1974.

Zoet, L. K. and Iverson, N. R.: A slip law for glaciers on deformable beds, Science, 368, 76–78, 2020.

Zwally, H. J., Giovinetto, M. B., Beckley, M. A., and Saba, J. L.: Antarctic and Greenland Drainage Systems, GSFC Cryospheric Sciences Laboratory, http://icesat4.gsfc.nasa.gov/cryo_data/ant_grn_drainage_systems.php (last access: 5 November 2025), 2012.

Zweng, M. M., Reagan, J. R., Seidov, D., Boyer, T. P., Locarnini, R., Garcia, H. E., Mishonov, A. V., Baranova, O. K., Weathers, K. W., Paver, C. R., and Smolyar, I. V.: World Ocean Atlas 2018, Volume 2: Salinity, Tech. Rep. Atlas NESDIS 82, NOAA, https://data.nodc.noaa.gov/woa/WOA18/DOC/woa18_vol2.pdf (last access: 14 October 2025), 2019.